Measurement of sound source intensity around a D-shaped cylinder by particle image velocimetry

Takayuki Yamagata [1]*, Yosuke Nakata [2], Nobuyuki Fujisawa [1]

[1] Flow Visualization Research Center, Niigata University, Niigata, Japan

[2] Graduate School of Science and Technology, Niigata University, Niigata, Japan

*yamagata@eng.niigata-u.ac.jp

Abstract

In this study, the sound source intensity around a D-shaped cylinder was measured by particle image velocimetry (PIV) based on Howe's vortex sound theory. The measurement of sound source intensity was conducted by using two sets of PIV system combined with the rotary shutter mechanism. The distribution of sound source intensity was varied with the angle of attack variation, which was in accordance with the microphone measurement of sound pressure level variation. The sound source intensity measurement revealed that the sound sources prevailed along the shear layer and in the rear region of the D-shaped cylinder.

1 Introduction

The reduction of aerodynamic noise generated in machinery such as vehicles, centrifugal fans, and wind turbines is an important subject for reduction in energy consumption and improvement of sound environment. The relation between sound source distribution and the flow structure is an important topic in designing low noise machinery. Several measurement techniques were proposed to measure the sound sources. Beam forming techniques identify the sound source but the information about relation between sound source and flow structure is limited (Cho et al., 2010). Correlation techniques of acoustic wave and a flow quantities obtained by particle image velocimetry (PIV) provide the information about the sound source generations, however, the results depend on the selected flow quantity for the correlation (Henning et al., 2008; Oguma et al., 2013). The techniques combining PIV and acoustic analogies have been also developed (Moor et al., 2011; Uda et al., 2011). The PIV-based techniques give both information of the sound source intensity and the flow structure but they require time-resolved (TR) PIV with rapid frame-rate camera systems to evaluate temporal derivatives of flow fields. Typically, the temporal resolution of the TR-PIV varies with the camera, while there is a trade-off between the temporal resolution and spatial resolution. In our former study, two sets of PIV system with pulse lasers were employed to obtain time derivatives of flow quantities from two instantaneous velocity fields with a short time interval (Oguma et al., 2016).

In this study, the sound source intensity was measured by particle image velocimetry (PIV) based on Howe's vortex sound theory. The measurement of the sound source intensity was applied for the flow around a D-shaped cylinder with various angles of attack.

2 Theoretical background

According to Howe's vortex sound theory, the sound pressure emitted from a bluff body can be expressed by using time-derivative of the vorticity and the velocity in the flow field. In the low Mach-number limit, the sound pressure P_a generated by a compact body is described as follows:

$$P_a(\mathbf{x}, t) = \frac{\rho_0 x_i}{4\pi c |\mathbf{x}|^2} \int_V I(\mathbf{y}, t) dV, \qquad (1)$$

where ρ_0 represents the fluid density, c represents the sound speed, $\mathbf{x}$ represents the position vector of the observer, $\mathbf{y}$ represents the position vector of sound sources, V represents the volume of interest, and I represents sound source intensity. The sound source intensity is expressed by using the Lamb vector $\boldsymbol{\omega} \times \boldsymbol{u}$ and velocity potential as follows:

$$I(\mathbf{y}, t) = \frac{\partial}{\partial t}(\boldsymbol{\omega} \times \boldsymbol{u})(\mathbf{y}, t - |\mathbf{x}|/c) \cdot \nabla Y_i, \qquad (2)$$

where $\boldsymbol{\omega}$ represents the vorticity, $\boldsymbol{u}$ represents the velocity vector, and Y_i represents the velocity potential. Assuming two-dimensional flow field around the bluff body, the sound source intensity could be evaluated from the time-derivative measurement of the velocity fields with PIV.

3 Experimental Methods

Measurement of sound source intensity was carried out for a flow around a D-shaped cylinder in a closed test section of a wind tunnel. The measurement section was covered by an anechoic chamber for aerodynamic sound measurement. The wind tunnel had a cross-section of 190 mm × 190 mm. The wind tunnel walls were made of acrylic resin for flow visualization purpose. The target D-shaped cylinder had a cross-section which combined a front circular surface and a rectangular back. The diameter of the round surface was $d = 15$ mm, and the streamwise length was $a = 15$ mm, so that the width-to-height ratio was $a/d = 1$. Details of the experimental wind tunnel and the D-shaped cylinder are the same as the former experiment (Yamagata et al., 2018). The free-stream velocity of the wind tunnel was $U_0 = 20$ m/s, therefore, the Reynolds number was $Re (= U_0 d/v) = 2 \times 10^4$, where v was the kinematic viscosity of air.

The sound pressure level of Aeolian tone emitted from the D-shaped cylinder was measured using a microphone, which had a diameter of 12.7 mm. The sound pressure was measured by a microphone located in the lateral direction from the cylinder with a distance of 130 mm. The top and bottom walls of the test section were replaced by urethane foam to minimize the reflection of the sound wave. The microphone had a flat frequency response ranging from 20 Hz to 8 kHz. The sampling rate was 10 kHz and the sampling time for the statistical evaluation was 30 s. The sound spectra were also evaluated using fast Fourier transform (FFT) analysis.

In order to measure the sound source distribution, the time-derivative of the velocity fields was measured by particle image velocimetry (PIV). The time-derivative measurement was carried out with two sets of standard PIV systems, which consisted of double-pulsed Nd: YAG lasers (70 mJ/pulse) and two charge coupled device (CCD) cameras (1280 × 1024 pixels with gray level of 12 bits). Figure 1 shows the layout of the experimental optics. The Scheimpflug configuration was employed for a camera to reduce the influence of the inclination of the camera. Figure 2 shows the timing chart of the cameras and lasers for the time-derivative PIV measurement. The CCD camera has a frame straddling function which enables to record two images with a short time interval. However, the exposure time of the second frame is longer than the time interval of the time-derivative measurement Δt_2. Therefore, illuminations for the second PIV
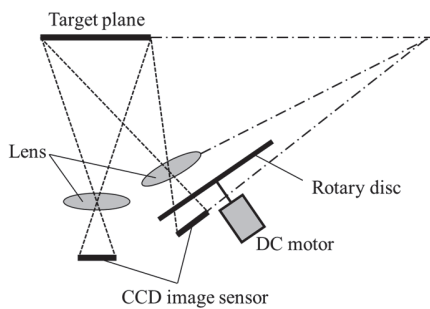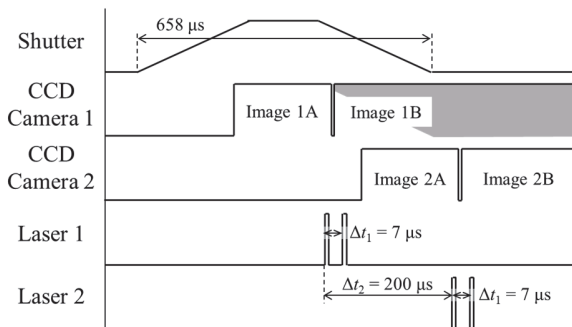

Fig. 1 Layout of experimental optics   Fig. 2 Timing chart of time-derivative PIV measurement

system were recorded in the second frame of the first PIV system. In order to avoid this extra illuminations, a mechanically rotational shutter (Tomimatsu et al., 2003) was developed and installed in front of the CCD camera for the first PIV system. The mechanical shutter was made of a rotating disk having a diameter of 190 mm with a slit of 10 mm width. The rotation speed of the shutter was controlled to be 3100 rpm by a speed controller. The rotation speed and the position of the slit was measured by a photoelectric sensor. The timing of the image recording and laser illumination was synchronized by a pulse generator. The other conditions for the PIV measurement were as follows. The size of the field of view was 48 × 38 mm². Oil smoke of 1 μm in diameter was employed as a tracer. A direct cross-correlation method with sub-pixel accuracy was employed for PIV analysis. The time interval of the PIV analysis was set to a value not to exceed the particle displacement of 4 pixels. The uncertainty of the PIV analysis was estimated to be 3%. The time interval for the time-derivative evaluation of the velocity fields was set to 200 μs.

4 Results and Discussion

Aerodynamic sound properties were investigated for the flow around a D-shaped cylinder with various angles of attack. Figure 3 shows variations of overall sound pressure level and Strouhal number with various angles of attack. Strouhal number ($St = fd'/U_0$) was evaluated from the peak frequency of the sound pressure spectrum, where d' represents projective length of the D-shaped cylinder in the streamwise direction. The D-shaped cylinder with zero angle of attack showed minimum sound pressure level. A local maxima of the sound pressure level was observed around $\alpha = 75°$ and $\alpha = 135, 150°$. A local minima were observed at $\alpha = 105°$ and $165°$. The largest sound pressure level was measured at $\alpha = 180°$. The sound pressure level of the D-shaped cylinder showed a similar tendency to that of a semi-circular cylinder (Yamagata et al., 2016). The Strouhal numbers were varied in a range of $St = 0.11 – 0.19$ in association with the change of the sound pressure level. Lower Strouhal numbers were observed at local peak sound pressure level. This implies that the large vortices were generated behind the cylinder and they created sound sources around the cylinder.

Flow fields around the D-shaped cylinder with various angles of attack were measured with a standard PIV technique. Figure 4 shows contours of velocity magnitude around the D-shaped cylinder at typical angles of attack. The D-shaped cylinder with $\alpha = 0°$ showed a large recirculating region behind the cylinder, since the flow separation occurred at rear edges. The flow separations of the case with $\alpha = 75°$ occurred at upside rear rounded surface and downside front edges. An asymmetric and wide recirculating region was produced behind the cylinder. A local peak sound pressure level was observed at this angle of attack. In the case of $\alpha = 105°$, the flow separation occurred at upside rear rounded surface and downside rear edge. The recirculating region became smaller than the case of $\alpha = 75°$ and the sound pressure level
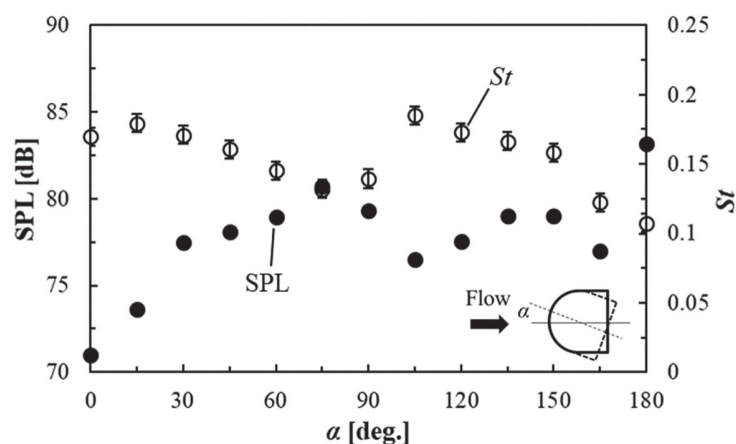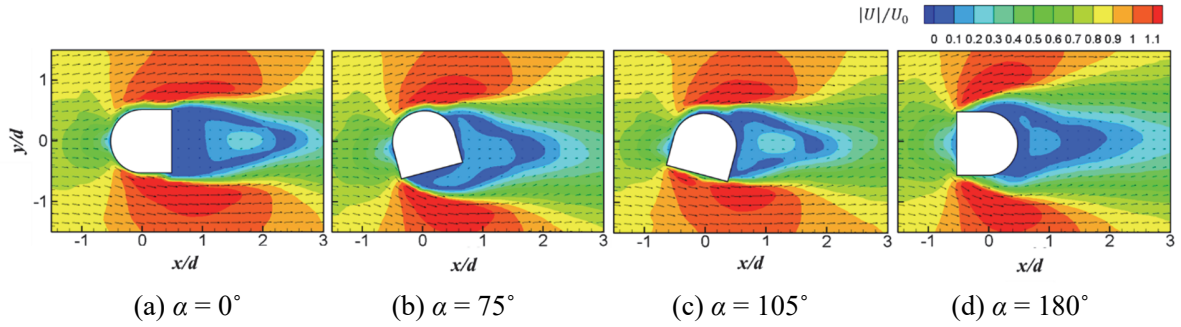

Fig. 3 Sound pressure level and Strouhal number

(a) $\alpha = 0°$ (b) $\alpha = 75°$ (c) $\alpha = 105°$ (d) $\alpha = 180°$

Fig. 4 Mean velocity fields around a D-shaped cylinder

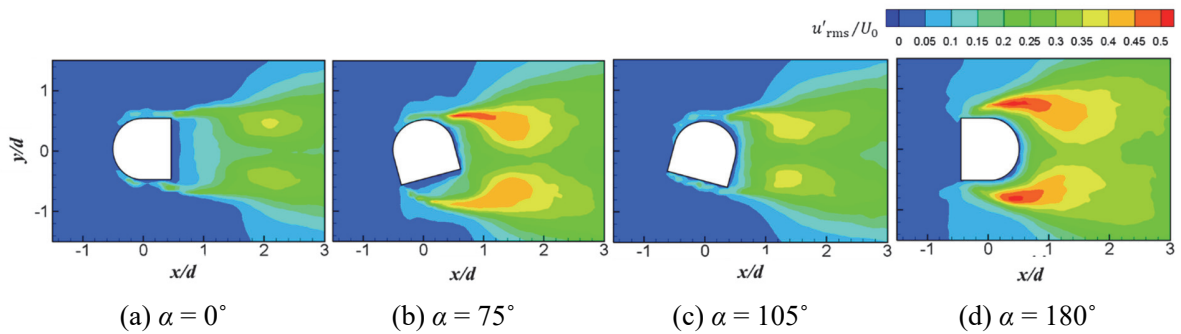(a) $\alpha = 0°$ (b) $\alpha = 75°$ (c) $\alpha = 105°$ (d) $\alpha = 180°$

Fig. 5 Contours of streamwise velocity fluctuations

was reduced at this angle. The flow separated at the front edges in the case of $\alpha = 180°$. Therefore, the wider wake width was observed behind the cylinder at $\alpha = 180°$.

Figure 5 shows the distributions of streamwise velocity fluctuations. The magnitude of the velocity fluctuations in the wake becomes large at $\alpha = 75°$ and $180°$, where the high sound pressure levels are observed in Fig.3. The velocity fluctuations were weak behind the cylinder with $\alpha = 0°$ and $105°$, at which the sound pressure level were smaller. The strong velocity fluctuations were observed near the shear layer at $\alpha = 75°$ and $180°$, at which the sound pressure level showed local maximum.

Sound source intensities around the D-shaped cylinder were measured by using the time-derivative PIV technique, while the velocity potential around the D-shaped cylinder in Eq. (2) was obtained numerically using OpenFOAM v4.1. Figure 6 shows instantaneous distributions of sound source intensities around the D-shaped cylinder at the typical angle of attack. The instantaneous sound source intensities distributed along the side walls at $\alpha = 0°$. The sound source detached from the sound source layer in the wake and the intensity became weak. In the case of $\alpha = 75°$, the sound source intensity can be seen near the shear layer region and near the back surface of the cylinder. The sound source intensity was reduced near the back surface in the case of $\alpha = 105°$. The strong sound source intensity was observed around the cylinder in the case of $\alpha = 180°$. The sound source existed along the side and back surfaces in this case.

Figure 7 shows root-mean-square (RMS) values of the sound source intensities. The strong fluctuations of the sound source intensity existed in the shear layer in all cases. The difference of the sound source fluctuations can be seen in the rear region of the cylinder. The fluctuations of the sound source intensity became weaker in the case of $\alpha = 0°$ and $105°$. The fluctuations of sound source intensity increased in the case of $\alpha = 75°$ and $180°$. These results showed that the fluctuations of the sound source intensity were in reasonable agreement with the noise measurement by microphone.

The fluctuations of the sound source intensity were integrated in the measured field to compare with the sound pressure level measured by the microphone. Figure 8 shows the variation of the integrated sound source intensity with angles of attack. The sound pressure level is also plotted for comparative purpose. The sound source intensity shows the same tendency as the sound pressure levels for the variation of the angle of attack. This result indicated the validity of the present measurement of the sound source intensity.
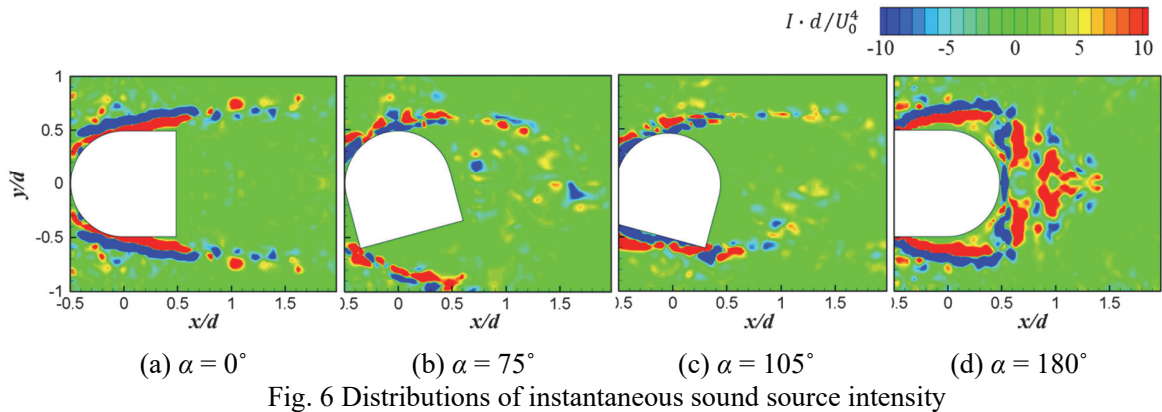
$I \cdot d / U_0^4$

-10   -5   0   5   10

(a) $\alpha = 0°$ (b) $\alpha = 75°$ (c) $\alpha = 105°$ (d) $\alpha = 180°$

Fig. 6 Distributions of instantaneous sound source intensity

$I'_{rms} \cdot d^2 / U_0^4$

0   20   40   60

(a) $\alpha = 0°$ (b) $\alpha = 75°$ (c) $\alpha = 105°$ (d) $\alpha = 180°$
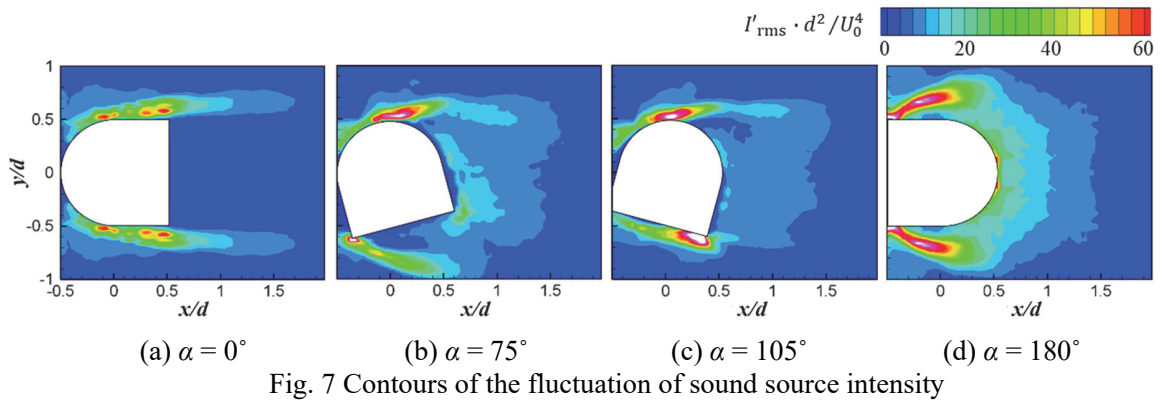
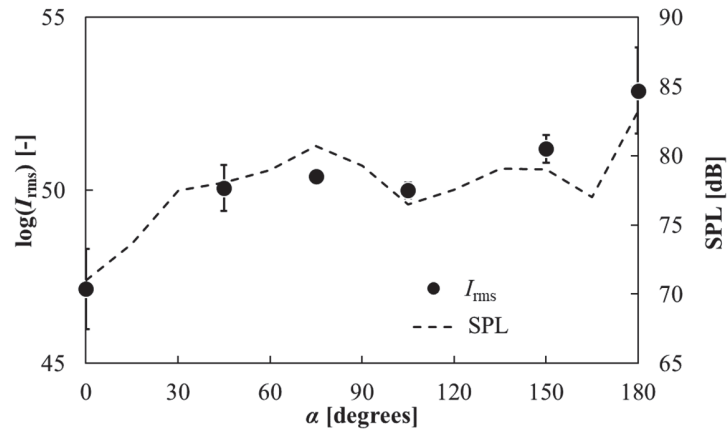Fig. 7 Contours of the fluctuation of sound source intensity

Fig. 8 Variation of sound source intensity with angles of attack

5 Conclusion

Fluctuations of sound source intensity around a D-shaped cylinder with variable angle of attack were measured by two sets of standard PIV systems combined with the rotary shutter mechanism. The fluctuations of the sound source intensity obtained from the time-derivative PIV measurement indicated a similar behavior to the microphone measurement, which indicated the validity of the sound source measurement by the time-derivative PIV. The magnitude of the fluctuation of the sound source intensity increased at a certain angles of attack and the results were in agreement with the sound pressure level

obtained from the microphone measurement. The high fluctuations of the sound source intensity were distributed along the shear layer and in the rear of the cylinder.

References

Cho T, Kim C, Lee D (2010) Acoustic measurement for 12% scaled model of NREL phase VI wind turbine by using beamforming. Current Applied Physics 10:5320-5325.

Henning A, Kaepernick K, Ehrenfried K, Koop L, Dillmann A (2008) Investigation of aeroacoustic noise generation by simultaneous particle image velocimetry and microphone measurements. Experiments in Fluids 45:1073-1085.

Howe MS (1975) Contribution to the theory of aerodynamic sound, with application to excess jet noise and the theory of the flute. Journal of Fluid Mechanics 71:625-673.

Moore P, Lorenzoni V, Scarano F (2011) Two techniques for PIV-based aeroacoustic prediction and their application to a rod-airfoil experiment. Experiments in Fluids 50:877-885.

Oguma Y, Yamagata T, Fujisawa N (2013) Measurement of sound source distribution around a circular cylinder in a uniform flow by combined particle image velocimetry and microphone technique. Journal of Wind Engineering and Industrial aerodynamics 118:1-11.

Oguma Y, Fujisawa N (2016) Sound source measurement of a semi-circular cylinder in a uniform flow by particle image velocimetry. Journal of Flow Control, Measurement & Visualization 4:162-170.

Tomimatsu S, Fujisawa N, Hosokawa A (2003) PIV measurement of Velocity Field in Spray Combustor. Journal of Visualization 6:273-281.

Uda T, Nishikawa A, Someya S, Iida A (2011) Prediction of aeroacoustic sound using the flow field obtained by time-resolved particle image velocimetry. Measurement Science and Technology 22:075402 (10 pages).

Yamagata T, Saito N, Fujisawa N (2016) Aeolian Tone from a Semi-circular Cylinder in a Stream. Journal of Flow Control, Measurement and Visualization 4:30-37.

Yamagata T, Saito N, Fujisawa N (2017) Experimental and numerical studies on Aeolian tone from D-shaped cylinder. Journal of Mechanical Engineering Science doi:10.1177/0954406217747912